coatings

MDPI

Article

Effects of Niobium Carbide Additions on Ni-Based Superalloys: A Study on Microstructures and Cutting-Wear Characteristics through Plasma-Transferred-Arc-Assisted Deposition

Kuan-Jen Chen [1,*] and Hung-Mao Lin [2,*]

[1] Department of Mechanical Engineering, Southern Taiwan University of Science and Technology, Tainan City 71005, Taiwan
[2] Department of Chemcial and Materials Engineering, Southern Taiwan University of Science and Technology, Tainan City 71005, Taiwan
* Correspondence: kjchen@stust.edu.tw (K.-J.C.); hmlin@stust.edu.tw (H.-M.L.); Tel.: +886-6-2533131-3529 (K.-J.C.); +886-6-2533131-3731 (H.-M.L.)

Abstract: This study applied plasma transferred arc (PTA) welding to fabricate hard cladding layers by using nickel-based superalloy (NCR7) and niobium carbide (NbC) powders as filler material. The resultant composite claddings were coated onto ductile iron and then analyzed to understand the effect of different quantities of NbC on the solidification structures of the cladding layers and on the characteristics of the interface between the cladding layers and the ductile iron. Cutting tests were also conducted to assess the morphology and mechanism of flank wear on PTA NbC/NCR7 composite cladding tools. The results revealed that the cladding specimens' microstructures comprised a mixture of dendrites and interdendritic eutectics along with a considerable quantity of carbides (MC, M7C3, and M23C6) scattered within the γ-Ni matrix. Incorporating considerable NbC carbide enhanced the claddings' surface hardness, but it had a limited effect on improving the flank wear on the turning tools. The flank wear on the composite cladding tools intensified as the NbC content was increased. The wear behavior, defined by brittle fractures and stripped NbC particles, led to a decline in turning tool performance. Accordingly, the Ni-based alloy composite cladding with larger NbC particles appears more suitable for sliding or erosion applications under normal stress conditions.

Keywords: plasma transferred arc; nickel-based superalloy; niobium carbide; dry-cutting; flank wear

check for updates

Citation: Chen, K.-J.; Lin, H.-M. Effects of Niobium Carbide Additions on Ni-Based Superalloys: A Study on Microstructures and Cutting-Wear Characteristics through Plasma-Transferred-Arc-Assisted Deposition. *Coatings* **2024**, *14*, 167. https://doi.org/10.3390/coatings14020167

Academic Editor: Andrew J. Pinkerton

Received: 8 January 2024
Revised: 25 January 2024
Accepted: 27 January 2024
Published: 28 January 2024

1. Introduction

Surface coatings are primarily designed to offer functional properties that differ from the inherent characteristics of the material surface and matrix, thus enhancing hardness, wear resistance, and corrosion resistance [1–3]. Machine parts that frequently come into contact with each other, such as gears, bearings, crankshafts, and molds, are often composed of high-toughness materials; these parts are subjected to surface coating to achieve both a tough matrix and a wear-resistant surface layer [4–6]. Ductile iron is a high-toughness material that exhibits considerable strength, heat resistance, and impact toughness; therefore, it is widely used in applications such as pressure pipes, automobiles, agricultural machinery, construction, and valves [7,8]. To improve its fatigue life, ductile iron is subjected to coating treatments that boost its resistance to wear, corrosion, and high-temperature oxidation.

Current metallurgical-bonding-based surface treatment processes for metals include discharge machining [9], electron beam coating [10], laser coating [11], and plasma transferred arc (PTA) welding [12,13]. Among these processes, PTA welding has gained favor for its efficient welding speed and superior weld quality [14]. PTA welding operates on the same principle as plasma arc welding (PAW) but uses alloy powder as filler material, thus offering more flexibility in alloy selection. Moreover, PTA welding produces a thicker cladding layer that bonds efficiently with the matrix, providing excellent resistance to high-temperature oxidation, corrosion, and wear [15,16]. PTA welding has considerable potential in the application of surface hardening. It is suitable for the covering of hard layers on the surface of materials with good ductility, moderate strength, and relatively cheap prices, thereby improving product profits and applicability.

Ni-based superalloys are frequently used as hard cladding materials in the PTA process [17]. Such alloys maintain a stable austenite structure at high temperatures owing to numerous secondary phases (MC, M23C6, M7C3 carbides) formed by the addition of various alloying elements, thereby improving their high-temperature strength [18]. In addition, they contain ordered intermetallic compounds (γ' or γ'') that are stable at high temperatures, thus contributing to their considerable creep resistance [19]. Therefore, Ni-based superalloys maintain high strength at high temperatures and exhibit excellent resistance against creep, fatigue, and corrosion, resulting in their extensive application in harsh environments. However, they exhibit poor wear resistance owing to their unique microstructures [20]. To solve this problem, several studies have proposed the addition of carbides into the Ni-based alloy coatings [21,22]. Among the various metal carbides, niobium carbide (NbC) as hard particles has a considerable potential to enhance Ni-based alloy coatings due to its high microhardness, excellent chemical stability, and good wear resistance [23]. In addition, little literature is available on NbC-reinforced Ni-based alloy composite coatings for PTA welding.

The present study used PTA welding to deposit NbC/Ni-based alloy composite powders onto the surface of ductile iron and then examined the role of NbC during solidification. To determine the effects of the NbC content on the wear resistance of the NCR-7 superalloy, this study conducted dry-cutting tests by shaping the composite cladding specimens into turning inserts—which were used as cutting tools—and using an ADC12 die-casting aluminum alloy as the workpiece. ADC12 alloys contain a considerable amount of Si, which can cause considerable wear and a built-up edge (BUE) [24], creating a severe wear environment. Accordingly, the study primarily explored the effects of NbC addition on the solidification structure, hardness, and phase composition of the composite cladding. The study also examined the flank wear characteristics of the turning tool after the cutting tests to clarify its failure mechanism.

2. Materials and Methods

This study used Ni-based alloy (NCR-7) powder and NbC powder as composite materials for PTA cladding. The NCR-7 alloy powder (particle size: 80–320 mesh) served as the matrix for the composite cladding material, and its chemical composition is presented in Table 1. The study then combined the NbC powder at weight ratios of 0, 30, and 50 wt.% with the NCR-7 alloy powder to create the composite cladding powder. Ductile iron specimens were obtained through sand-casting, and its chemical composition is presented in Table 2. Machined ductile iron specimens, each measuring 90 mm × 25 mm × 15 mm, were used as the PTA cladding substrates (Figure 1a). To evaluate the effects of plasma energy on the structural characteristics of the cladding layer, this study fabricated NCR-7 superalloy specimens by using different arc currents. The PTA cladding parameters are detailed in Table 3.

Table 1. Chemical composition of Ni-based alloy powder (wt.%).

	Cr	C	Si	B	Ni
NCR-7	19.0	0.95	4.7	3.5	Bal.

Table 2. Chemical composition of ductile iron specimen (wt.%).

C	Si	Mn	P	S	Cr	Cu	Mg	Fe
3.50	2.78	0.32	0.01	0.015	0.21	0.60	0.03	Bal.

Table 3. Experimental conditions for PTA cladding and cut testing.

PTA cladding	Powder flux	2400 g/h
	Plasma gas (Ar)	4 L/min
	Powder delivery gas (Ar)	3 L/min
	Shielding gas (Ar)	24 L/min
	Overlay current	100–140 A
	Overlay voltage	32 V
	Travel speed	80 mm/min
	Nozzle vibration	70 times/min
Cut testing	Cutting speed	200 m/min
	Feed rate	0.01 mm/rev
	Cutting depth	0.5 mm

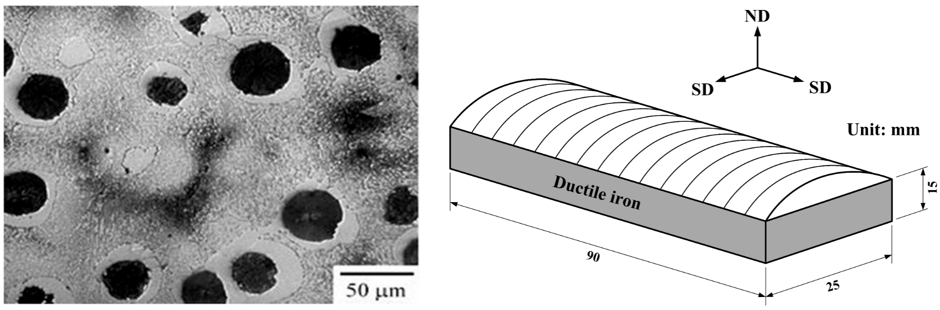

(**a**) (**b**)

Figure 1. (**a**) Microstructure of ductile iron. (**b**) Dimensions of PTA cladding specimen.

To investigate the wear behavior of the NCR-7 superalloy at high temperatures, dry-cutting tests were conducted. The composite cladding specimens (Figure 1b) were shaped into turning inserts measuring 12.5 mm × 12.5 mm × 9 mm; these inserts were used as the cutting tools in the tests. Moreover, an ADC12 aluminum alloy rod (Φ: ~40 mm) was used as the workpiece in the cutting tests. The following parameters were used in the cutting tests: cutting speed, 200 m/min; feed rate, 0.01 mm/rev; and cutting depth, 0.5 mm (Table 3). Each turning insert was used to cut a fixed distance (300, 600, 900, and 1200 m) into the workpiece, after which it was immersed in a 10% NaOH aqueous solution for 2 h to remove any BUE. Subsequently, the inserts were cleaned with acetone in an ultrasonic machine, and the resulting flank wear was then assessed.

The superalloy specimens were etched with 5% Nital etchant, and their microstructures were then observed through optical microscopy (OM). The specimens' phase compositions were examined using X-ray diffraction (XRD), and their hardness values were estimated through hardness tests. Rockwell hardness tests were conducted to measure the surface hardness of the cladding specimens. The microhardness distribution from the ductile iron matrix to the cladding layer was determined at 0.25 mm intervals by using the Vickers microhardness test with a 100 g load for 15 s. In addition, a depth profile analysis was conducted for the PTA cladding specimens using scanning electron microscopy/energy dispersive X-ray spectroscopy (SEM-EDS). Finally, after the cutting tests, the flank wear and subsurface morphologies of the tested inserts were observed using OM and SEM to confirm the role of NbC addition.

3. Results and Discussion

3.1. Evolution of Solidification Microstructures and Hardening Ability in NCR-7 with NbC Addition

This study explored the effects of the arc current on the hardness evolution of the NCR-7 cladding specimens, and the corresponding results are presented in Figure 2. The specimens' hardness values decreased as the arc current was increased (Figure 2a), indicating that all specimens had high surface hardness values at low arc current levels [25]. The plasma overlay current influenced the agglomeration and growth of the PTA cladding structures [26] in addition to influencing the degree of thermal interaction between the matrix and the cladding layer [27]. Moreover, the microhardness distribution from the ductile iron matrix to the clad layer is illustrated in Figure 2b. The microhardness measurement results revealed that the average microhardness of the NCR-7 overlayer was 900 HV and that the microhardness changed significantly in interfacial regions, indicating notable thermal effects during PTA cladding. The average microhardness of the NCR-7 overlayer slightly decreased with the increase in arc current. In addition, the dilution effect caused by higher arc current caused a non-homogeneous overlayer, thus affecting the wear resistance of the cladding layer. On the basis of these results, this study investigated wear resistance by fabricating NCR-7 superalloys with different NbC content levels under a low arc current.

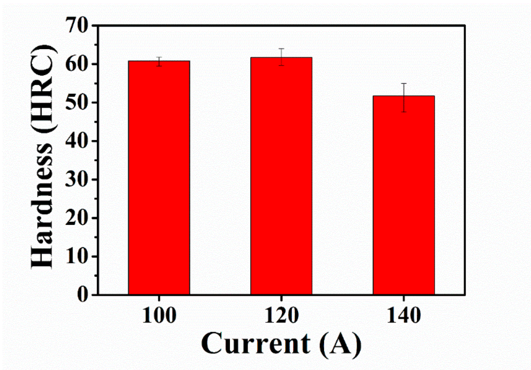

(**a**)

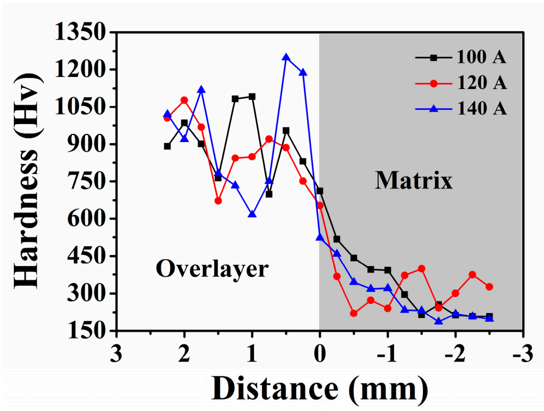

(**b**)

Figure 2. (**a**) Surface hardness of NCR-7 cladding specimen and (**b**) hardness of NCR-7 cladding specimens in SD direction under different arc currents.

Figure 3 illustrates the microstructures of the PTA cladding specimens with different NbC content levels. The NCR-7 specimens exhibited a uniform microstructure with dendrites and a fine interdendritic eutectic mixture (size: 3–5 μm). The cladding layer without NbC had a relatively pronounced quantity of dendrites (Figure 3a). However, in the cladding layer with 30 and 50 wt.% NbC powder (Figure 3b and 3c, respectively), the powder did not melt fully in the PTA welding process; therefore, the quantity of dendrite structures decreased significantly, resulting in the distribution of a considerable quantity of NbC particles in the matrix. Notably, numerous fine, dark particles adhered to the NbC particle surfaces. According to the literature, NbC particles could provide nucleation sites for chromium diboride (CrB) phases in a molten matrix [23]. Therefore, the fine dark particles observed in the present study could be associated with hardening phases such as CrB or related carbides. Accordingly, the effects of NbC content on the compositions of Ni-based superalloy composite specimens warrant further investigation.

(**a**) (**b**) (**c**)

Figure 3. Microstructures of NCR-7 specimen with various NbC powder content levels: (**a**) 0, (**b**) 30, and (**c**) 50 wt.%.

Figure 4 depicts SEM images of the PTA cladding specimens. The results revealed that the specimens exhibited elongated dendrites that primarily contained Cr and C in addition to containing a small quantity of Ni and a considerable quantity of Fe (Figure 4a), which corresponded to MC carbides. Conversely, the interdendritic eutectic mixture was observed to contain an abundant quantity of Ni along with smaller quantities of Cr, Si, O, and C [28]. Notably, both the dendrites and the interdendritic eutectic mixture contained a considerable proportion of Fe, and this can be attributed to the dilution effect induced by the PTA welding process, which caused the thermal diffusion of Fe from the ductile iron matrix to the cladding layer. In this metallurgical context, Ni and Fe formed a Ni–Fe solid solution (γ-Ni) [29]. Thus, these MC carbides contained a small quantity of γ-Ni phases, and the granular eutectic mixture primarily consisted of γ-Ni phases with various carbides. This indicates a nonuniform alloy solution due to rapid, nonequilibrium solidification. Adding NbC to the superalloy specimen modified the size and shape of the MC carbides after solidification (Figure 4b,c). Large, blocky carbides were observed, and they corresponded to the NbC powder, which also contained considerable B content and trace Ti amounts; this can be attributed to the NbC–TiB2 composites formed during high-temperature PTA welding [30]. The presence of high-hardness NbC powder in the cladding layer matrix improved its wear resistance [31], and the NbC–TiB2 composites such as TiB2—an extremely hard ceramic compound with excellent wear resistance and oxidation stability—enhanced the wear characteristics of the Ni-based superalloy.

Figure 5 displays the phase compositions of the PTA cladding specimens with different NbC content levels. All superalloy specimens presented distinct diffraction peaks of (111) and (200) corresponding to a γ-Ni phase [32]. In addition, the specimens presented diffraction peaks corresponding to Cr7C3, Cr23C6, and CrB phases [26,33]. When NbC was added to the NCR-7 specimens, the (111), (200) diffraction peak intensity of the γ-Ni phase changed considerably, suggesting that a decrease in the NCR-7 proportion engendered a decrease in this peak. The (111) NbC phase orientation was the predominant factor contributing to the diffraction peaks corresponding to the carbide phases in the PTA cladding specimens [34], indicating that the NbC present in the composite powders was not completely remelted into the Ni-based superalloy. Figure 6 presents the elemental distribution profiles along the transverse section of the NCR-7 alloy and NCR-7 alloy composite cladding specimens supplemented with the NbC powder. This study measured the semiquantitative compositions of the subsurfaces of the PTA cladding specimens; in these measurements, the interface region was set to 0 and the cladding layer was directed forward. The distribution characteristics of the elements could be divided into three regions:

the cladding layer, the heat-affected zone (HAZ), and the ductile Fe substrate. The cladding layer contained a considerable quantity of Nb, and as the NbC content was increased, the Ni content decreased. This decrease was noted to be similar to the decrease in the γ-Ni phase intensity observed in the XRD patterns. Hence, the cladding layer matrix contained a considerable quantity of Nb, which could engender increased surface hardness due to dispersion strengthening. Fe diffusion into the cladding layer occurred in all specimens, which can be attributed to PTA-welding-induced dilution. The specimen with NbC addition exhibited an enhanced dilution effect, signifying a wider HAZ. However, the specimen with 50 wt.% NbC contained a relatively low Fe content within the cladding layer, suggesting excessive addition of NbC. Furthermore, NbC addition influenced the B and Cr quantities in the cladding layer. Accordingly, the formation of fine carbides (hardening phases) may alter the wear characteristics of the cladding layer [35].

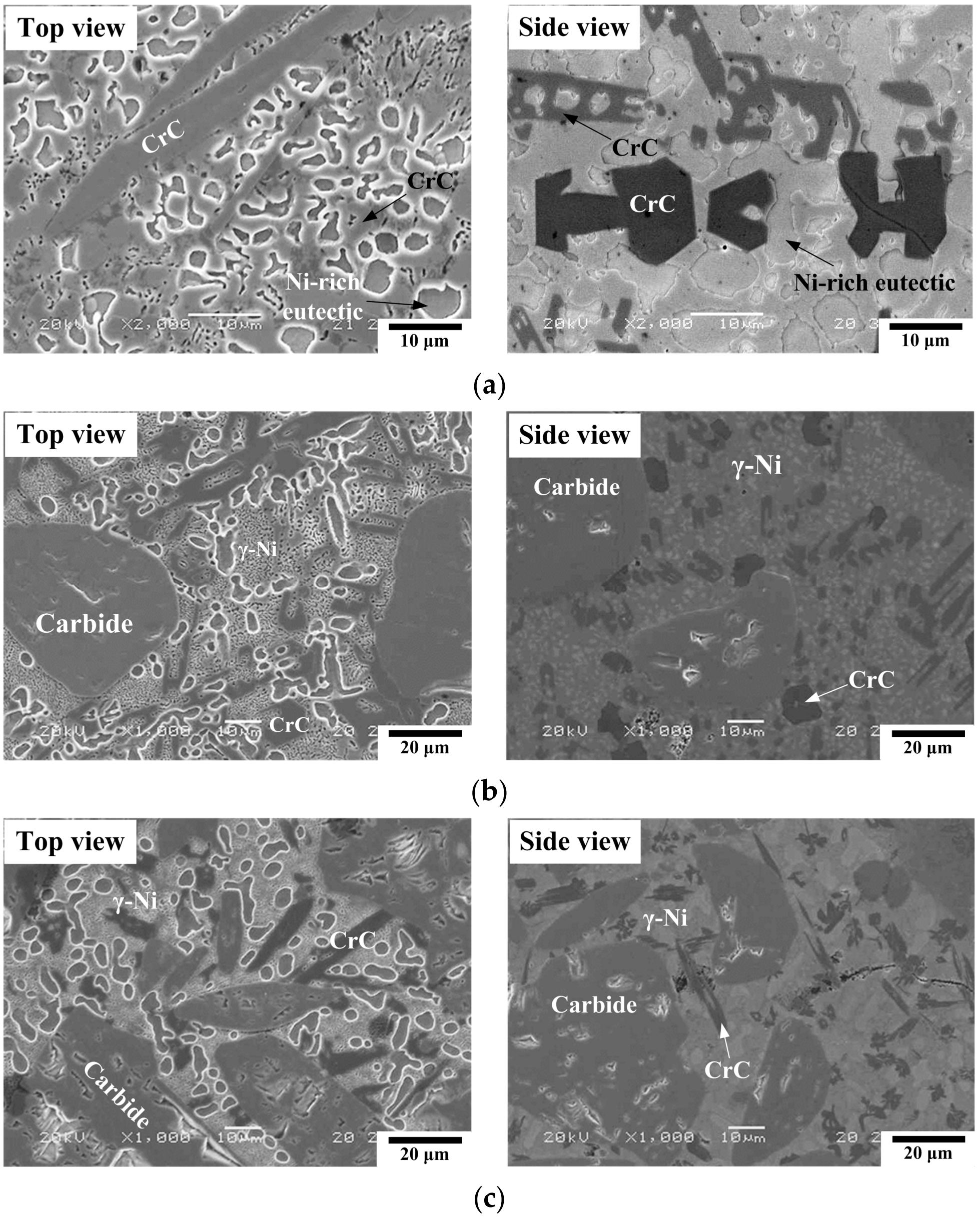

Figure 4. SEM images of NCR-7 specimen with various NbC powder content levels: (**a**) 0, (**b**) 30, and (**c**) 50 wt.%.

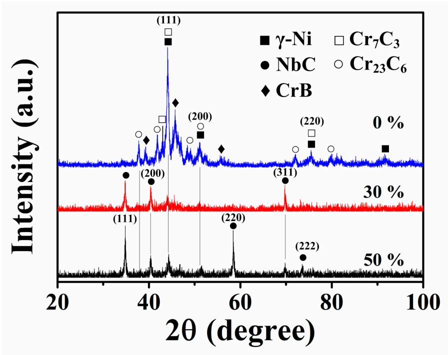

Figure 5. XRD patterns of PTA composite cladding specimens.

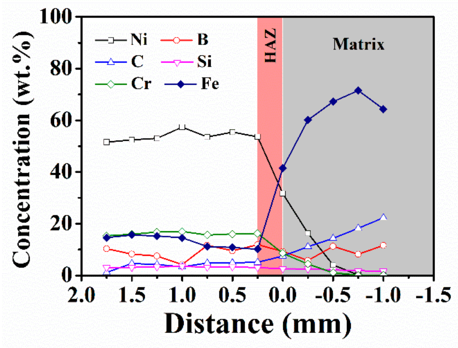

(**a**)

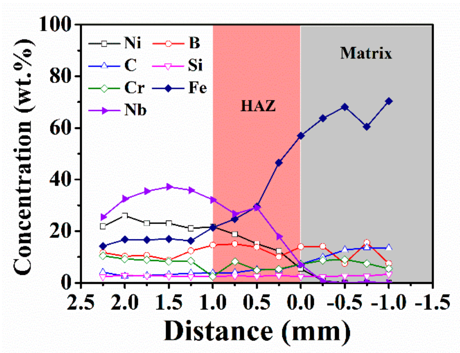

(**b**)

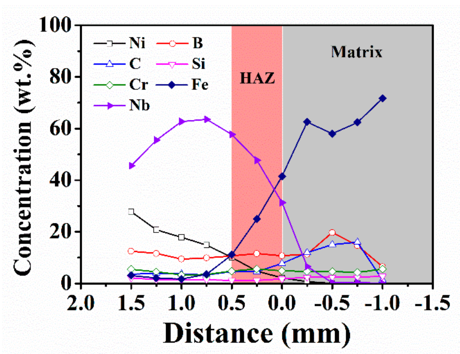

(**c**)

Figure 6. Depth profile of PTA cladding specimen with various NbC powder content levels: (**a**) 0, (**b**) 30, and (**c**) 50 wt.%.

3.2. Effects of NbC Addition on Cutting-Wear Characteristics of Cladding Layer

A previous study indicated that adding NbC could increase structural stress and fragility in a coating layer, thus engendering reduced wear resistance [36]. Because the wear mechanism of NbC-reinforced composite coating layers can be influenced by microstructural features and wear conditions, this study investigated the effects of NbC addition on the cutting-wear resistance of the cladding layer. Figure 7 depicts images of the flank wear on the cutting tool with NCR-7 cladding after various cutting distances. During the cutting tests, aluminum adhered to the flank cutting tool, forming a BUE [37]. As the cutting distance and temperature increased, the BUE accumulation intensified (Figure 7b). To understand the effect of NbC addition on flank wear, the BUE was removed using 3% Nital solution.

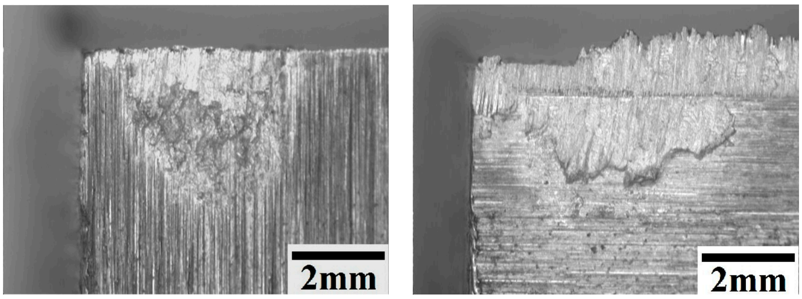

(**a**) (**b**)

Figure 7. Images of flank wear observed on NCR-7 cladding tools after different cutting distances: (**a**) 300 and (**b**) 1200 m.

Figure 8 depicts microscopic observations of flank wear on composite cladding specimens with different NbC content levels after a cutting distance of 1200 m. The NCR-7 cladding specimen without NbC exhibited normal wear characteristics on its upper edge (Figure 8a). However, after the incorporation of NbC (30 and 50 wt.%), the cutting tools exhibited triangular wear patterns (Figure 8b,c). Notably, the composite cladding specimen with high NbC addition has higher surface hardness, but it has a considerable wear width after the cutting test. As the NbC content was increased, the degree of flank wear became more pronounced, leading to an increased wear width. This result may be attributed to the cladding tool in the side direction undergoing a larger stress during the cutting process. To understand the relationship between tool life and wear behavior, the study measured the tools' wear width. In general, cutting conditions directly affect the type of flank wear surface formed. According to the JIS B 4011 specifications [38], a relatively uniform wear surface indicates normal wear, and the width of such wear can be estimated by calculating the average value of flank wear. Moreover, an irregular or triangular wear surface indicates abnormal wear, and the width of such wear can be estimated by calculating the maximum wear value (Figure 9).

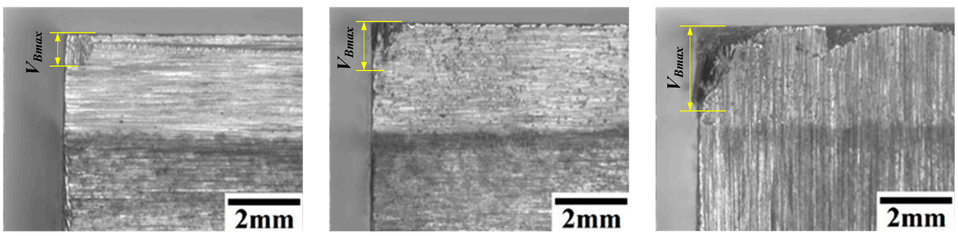

(**a**) (**b**) (**c**)

Figure 8. Microscopic images of flank wear on the composite cladding tools with different NbC content levels obtained after cutting tests of 1200 m: (**a**) 0, (**b**) 30, and (**c**) 50 wt.%.

Figure 10 illustrates plots of the degree of flank wear on the composite cladding tools with different NbC content levels as a function of cutting distance. According to the ISO 3685:1993 definition of tool life [39], an average wear value (VB) of >0.3 mm or a maximum wear value (VBmax) of >0.6 mm indicates that a tool has reached the end of its life. In this study, the degree of flank wear increased as the NbC content was increased, indicating that the addition of NbC did not improve cladding layer wear resistance. The NCR-7 cladding tool without NbC reached its life limit after the cutting distance exceeded 800 m. However, the tool with 30 wt.% NbC approached its life limit at the beginning (300 m) of the cutting tests. This study initially expected that the distribution of NbC within the cladding layer could enhance its wear resistance by forming a wear-resistant skeleton [40]. However, the addition of excess NbC increased structural stress and brittleness in the cladding layer, thereby reducing its wear resistance [36].

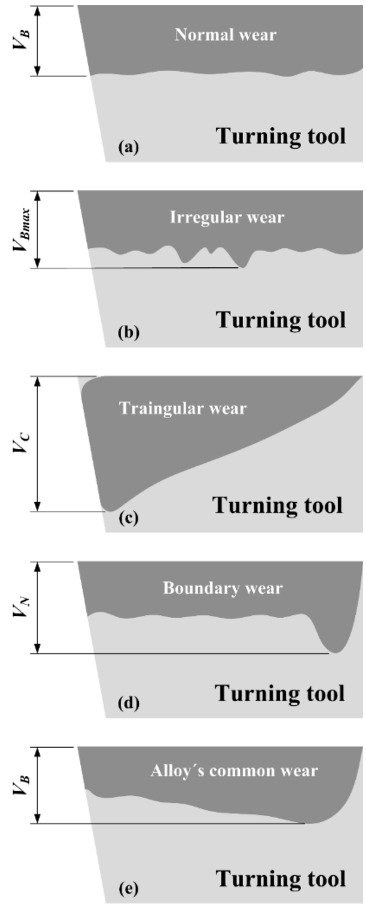

Figure 9. Patterns of flank wear: (**a**) normal wear, (**b**) irregular wear, (**c**) triangular wear, (**d**) boundary wear, and (**e**) alloy's common wear.

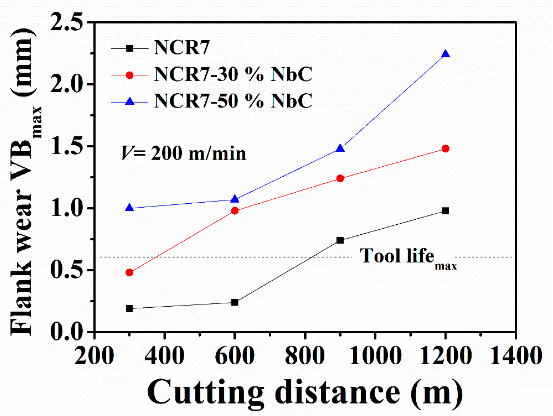

Figure 10. Flank wear observed on composite cladding tools with different NbC content levels as a function of cutting distance.

This study explored the relationship between NbC content and wear types by examining the surface morphology of the flank wear observed for each composite cladding tool after a 1200 m cutting distance (Figure 11). All composite cladding tools exhibited similar flank wear morphologies, which were predominately characterized by plastic grooves and surface polish. The presence of the plastic grooves suggested that plastic wear was the primary wear mechanism in the cutting tests. The formation of these grooves was attributed to ploughing and microcutting processes; ploughing resulted in the formation of raised portions on the workpiece surfaces, but these portions could be dislodged through repeated abrasion stress (Figure 11). This study determined that the mechanism underlying flank wear could involve cutting-induced material removal and plough-induced fatigue damage through repeated plastic deformation. In addition, brittle fractures within the microstructures could lead to wear, especially in brittle materials. In this context, the addition of carbides could reduce the wear resistance of the cladding layer, possibly due to the NbC carbides detaching from the cladding layer during the cutting process.

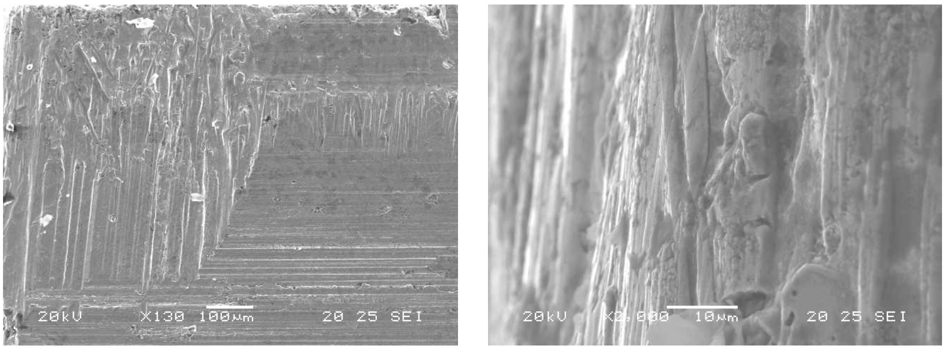

(**a**)

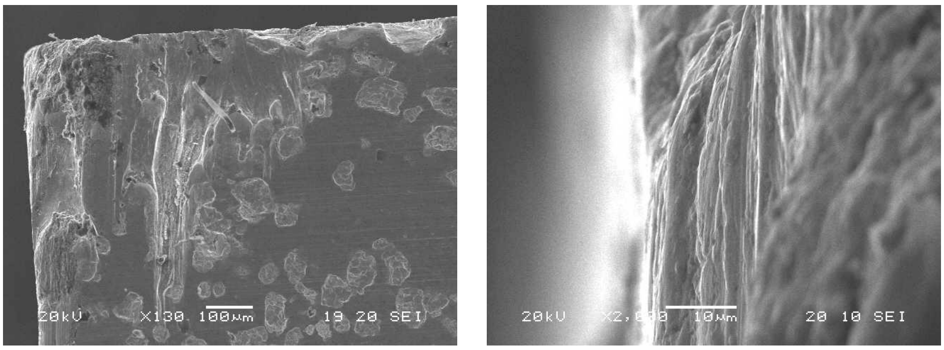

(**b**)

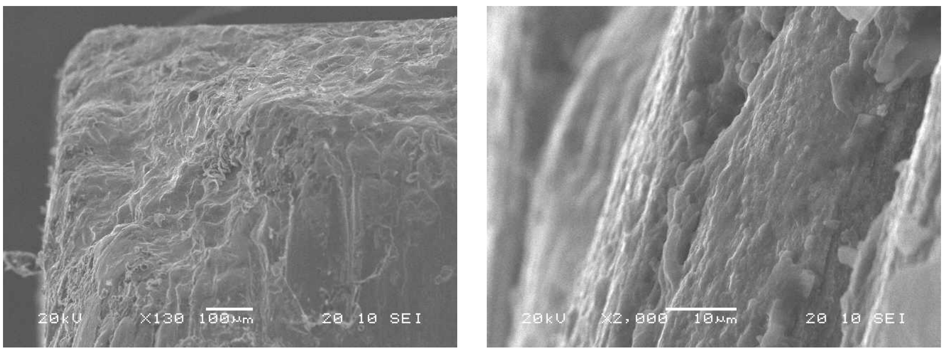

(**c**)

Figure 11. SEM images of flank wear on the composite cladding tools with different NbC content levels: (**a**) 0, (**b**) 30, and (**c**) 50 wt.%.

4. Conclusions

(1) The PTA-fabricated NCR-7 specimens exhibited uniform microstructures composed of dendrites and interdendritic eutectic mixtures. The NCR-7 microstructures were primarily composed of γ(Ni, Fe), Cr7C3, Cr23C6, and CrB phases, which contributed to the specimens' considerable hardness, indicating that the specimens can be used in wear-resistant coating applications.

(2) Mixing NbC powder with NCR-7 powder introduced NbC hardening particles to the matrix of the PTA composite cladding. Compared with the NCR-7 specimen without NbC, the composite claddings with 30 and 50 wt.% NbC exhibited greater surface hardness due to dispersion strengthening. An analysis of interfacial elements revealed a substantial dilution effect caused by the thermal energy introduced in PTA welding. The composite claddings with NbC addition had considerable Nb content and a wider HAZ.

(3) Cutting tests revealed that the flank wear observed on the composite cladding tools exhibited a triangular wear morphology, which intensified as the NbC content was increased. The composite cladding tools with high NbC content exhibited failure at the beginning (300 m) of the cutting tests. The composite cladding tools composed of an excessive quantity of hardened NbC particles were prone to fracture due to stress concentration during the cutting tests. Thus, brittle fractures within the microstructures of the cladding tools directly shortened the lifespan of the tools. In addition, the study determined that material removal and fatigue wear during cutting contributed to the functional failure of the tools.

Author Contributions: Conceptualization, H.-M.L.; methodology, H.-M.L.; investigation, K.-J.C. and H.-M.L.; resources, H.-M.L.; writing—original draft preparation, K.-J.C.; writing—review and editing, K.-J.C.; funding acquisition, H.-M.L.; All authors have read and agreed to the published version of the manuscript.

Funding: This research received financial support from the National Science and Technology Council, Taiwan.

Informed Consent Statement: Not applicable.

Data Availability Statement: Data are contained within the article.

Acknowledgments: The authors are grateful to the National Science and Technology Council, Taiwan.

Conflicts of Interest: The authors declare no conflicts of interest.

References

1. Qu, X.Y.; Huang, H.; Wan, T.; Hu, L.; Yu, Z.L.; Liu, Y.J.; Dou, A.C.; Zhou, Y.; Su, M.R.; Peng, X.Q.; et al. An integrated surface coating strategy to enhance the electrochemical performance of nickel-rich layered cathodes. *Nano Energy* **2022**, *91*, 106665. [CrossRef]
2. Hu, Y.J.; Wang, Z.X.; Pang, M. Effect of WC content on laser cladding Ni-based coating on the surface of stainless steel. *Mater. Today Commun.* **2022**, *31*, 103357. [CrossRef]
3. Günen, A.; Soylu, B.; Karakaş, Ö. Titanium carbide coating to improve surface characteristics, wear and corrosion resistance of spheroidal graphite cast irons. *Surf. Coat. Technol.* **2022**, *437*, 128280. [CrossRef]
4. Pham, T.H.N.; Nguyen, V.T. Microstructure and micro-hardness of Al2O3-TiO2 coating by plasma spraying on SKD61 steel. *Mater. Trans.* **2020**, *61*, 1829–1832. [CrossRef]
5. Thompson, F.C.; Kustas, F.M.; Crawford, G.A. Oil-lubricated sliding wear performance of TiSiCN-coated ductile iron. *Wear* **2023**, *514–515*, 204567. [CrossRef]
6. Karthick, M.; Pavithra, E.; Cep, R.; Elangovan, M. Machining of custom-450 grade stainless steel using TiAlSiN-coated tungsten carbide tool inserts. *Processes* **2023**, *11*, 1037. [CrossRef]
7. Zhu, Y.X.; Keoleian, G.A.; Cooper, D.R. A parametric life cycle assessment model for ductile cast iron components. *Resour. Conserv. Recycl.* **2023**, *189*, 106729. [CrossRef]
8. Wang, B.X.; Qiu, F.; Barber, G.C.; Pan, Y.M.; Cui, W.W.; Wang, R. Microstructure, wear behavior and surface hardening of austempered ductile iron. *J. Mater. Res. Technol.* **2020**, *9*, 9838–9855. [CrossRef]
9. Guo, C.X.; Wang, X.; Xie, W.L.; Lai, S. Surface modification of aluminum alloy by wire electrical discharge machining with SiC nanofluid dielectric. *Int. J. Adv. Manuf. Technol.* **2023**, *127*, 3525–3536. [CrossRef]

10. Grenadyorov, A.S.; Solovyev, A.A.; Yakovlev, E.V.; Glukhov, I.A.; Semin, V.O.; Popova, N.A.; Solovyov, A.V. Ti-based surface alloy formed on AISI 316L austenite steel surface using low-energy high-current electron beam. *J. Alloys Comp.* **2023**, *955*, 170243. [CrossRef]
11. Chen, W.J.; Cai, Q.; Luo, Z.Y.; Wu, Y.B. Influence of heat treatment on strength and toughness of laser cladding iron-based coatings. *Mater. Lett.* **2023**, *335*, 133733. [CrossRef]
12. Chen, K.J.; Hung, F.Y.; Lui, T.S.; Shih, Y.R. Wear inducing phase transformation of plasma transfer arc coated tools during friction stir welding with Al alloy. *J. Eng.* **2019**, *2019*, 6413608. [CrossRef]
13. Xiao, B.T.; Yan, X.F.; Jiang, W.M.; Fan, Z.T.; Huang, Q.W.; Fang, J.; Xiang, J.H. Comparative study on the hardness and wear resistance of the remelted gradient layer on ductile iron fabricated by plasma transferred arc. *Metals* **2022**, *12*, 644. [CrossRef]
14. Guo, X.H.; Zhang, P.; Li, H.; Wang, M.Y. Design and performance of nitrogen-alloyed iron-based coating for enhancing galling resistance by plasma transferred arc welding. *Mater. Lett.* **2023**, *346*, 134535. [CrossRef]
15. Wang, R.D.; Ye, S.X.; Xie, Z.Y.; Zhang, Z.H.; Han, H.S.; Hong, J.G.; Zhang, Y.W.; Li, G.S.; Wu, W.H.; Lu, X.G. Effect of copper oxides on defect formation during PTA cladding of Stellite 6 on copper substrates. *Surf. Coat. Techonl.* **2023**, *466*, 129625. [CrossRef]
16. Lopez, X.A.; Munoz-Arroyo, R.; Hernandez-Garcia, F.A.; Alvarez-Vera, M.; Mtz-Enriquez, A.I.; Diaz-Guillen, J.C.; Flores, I.G.; Betancourt-Cantera, J.A.; Hdz-Garcia, H.M. Processing of Co-base/C-nanotubes compound coating on D2 steel using plasma transferred by arc: Tribological and mechanical performance. *Surf. Coat. Techonl.* **2023**, *461*, 129458. [CrossRef]
17. Wang, H.P.; Sun, R.X.; Zhang, M.Q.; Gou, B.; Mo, J.L. Impact-sliding behavior of Ni-based coating prepared on tunnel boring machine disc cutter material produced using a plasma transferred arc welding process. *Surf. Coat. Technol.* **2022**, *442*, 128186. [CrossRef]
18. Witte, J.; Huebler, D.; Schroepfer, D.; Boerner, A.; Kannengiesser, T. Wear behavior of innovative niobium carbide cutting tools in ultrasonic-assisted finishing milling. *Wear* **2023**, *522*, 204722. [CrossRef]
19. Gao, Q.; Zhang, L.Q.; Liu, J.Y.; Lin, J.P. Microstructure and mechanical properties of high nibium beta-gamma TiAl and IN718 alloy joints diffusion bonded by spark plasma sintering. *Intermetallics* **2022**, *151*, 107745. [CrossRef]
20. Huang, Z.Y.; Hou, Q.Y.; Wang, P. Microstructure and properties of Cr3C2-modified nickel-based alloy coating deposited by plasma transferred arc process. *Surf. Coat. Technol.* **2008**, *202*, 2993–2999. [CrossRef]
21. Haldar, V.; Pal, S. Influence of fusion zone metallurgy on the mechanical behavior of Ni-based superalloy and austenitic stainless steel dissimilar joint. *J. Mater. Eng. Perform.* **2023**, *64*. [CrossRef]
22. Lemos, G.; Fredel, M.C.; Pyczak, F.; Tetzlaff, U. Creep resistance improvement of a polycrystalline Ni-based superalloy via TiC particles reinforcement. *Mater. Sci. Eng. A* **2022**, *854*, 143821. [CrossRef]
23. Gang, D.; Biao, Y.; Qilin, D.; Ting, Y. Microstructure and wear resistance of in situ NbC particles reinforced Ni-based alloy composite coating by laser cladding. *J. Wuhan Univ. Technol.-Mater. Sci. Ed.* **2012**, *27*, 231–236. [CrossRef]
24. Ficici, F.; Keser, M. Effect of casting modification materials on cutting forces of an Al12Si alloy used in aircraft technology. *Mater. Test.* **2023**, *65*, 616–628. [CrossRef]
25. Fernandes, F.; Ramalho, A.; Loureiro, A.; Cavaleiro, A. Wear resistance of a nickel-based coating deposited by PTA on grey cast iron. *Int. J. Surf. Sci. Eng.* **2012**, *6*, 201–213. [CrossRef]
26. Xu, H.M.; Huang, H.H.; Liu, Z.F. Influence of plasma transferred arc remelting on microstructure and properties of PTAW-deposited Ni-based overlay coating. *J. Therm. Spray Technol.* **2021**, *4*, 946–958. [CrossRef]
27. Chan, W.S.; Lui, T.S.; Chen, L.H. Solidification structures in overlaying of cobalt-based superalloy on ferritic spheroidal graphite cast irons by plasma transferred arc process. *Mater. Trans.* **1996**, *37*, 50–55. [CrossRef]
28. Cai, S.P.; Liu, Y.F.; Song, Z.K.; Lu, F.G.; Wu, Z.; Xie, M.Z. Design, preparation, microstructure and tribological properties of Cr7C3 and CrxSy reinforced composite coating. *Wear* **2023**, *526–527*, 204955. [CrossRef]
29. Demirskyi, D.; Sakka, Y.; Vasylkiv, O. High-temperature reactive spark plasma consolidation of TiB2-NbC ceramic composites. *Ceram. Int.* **2015**, *41*, 10828–10834. [CrossRef]
30. Wang, J.G.; Zhang, Q.K.; Shen, W.J.; Liang, Z.M.; Chang, C.Q.; Yang, L.Y.; Li, J.H.; Huang, F.S. Failure analysis of a chromium plating layer on a piston rod surface and the study of Ni-based composite coating with Nb addition by laser cladding. *Metals* **2022**, *12*, 1194. [CrossRef]
31. Evangeline, A.; Sathiya, P. Dissimilar Cladding of Ni–Cr–Mo Superalloy over 316L Austenitic Stainless Steel: Morphologies and Mechanical Properties. *Met. Mater. Int.* **2021**, *27*, 1155–1172. [CrossRef]
32. Pizzatto, A.; Teixeira, M.F.; Rabelo, A.; Falcade, T.; Scheid, A. Microstructure and wear behavior of NbC-reinforced Ni-based alloy composite coatings by laser cladding. *Mater. Res.* **2021**, *23*, e20200447. [CrossRef]
33. Katea, S.N.; Tai, C.W.; Ström, P.; Larsson, P.O.; Vidarsson, H.; Westin, G. Niobium carbide—Nickel-niobium alloy composites from a nickel coated powder: Microstructural development during sintering. *Open Ceram.* **2021**, *6*, 100096. [CrossRef]
34. Shi, B.M.; Hung, S.M.; Zhu, P.; Xu, C.G.; Zhang, T.F. Microstructure and wear behavior of in-situ NbC reinforced composite coatings. *Materials* **2020**, *13*, 3459. [CrossRef]
35. Wang, H.; Song, X.; Wei, C.; Gao, Y.; Guo, G. Abrasion Resistance Enhancement of Ultrafine-structured WC-Co Coating Fabricated by using in situ Synthesized Composite Powder. *J. Mater. Sci. Technol.* **2013**, *29*, 1067–1073. [CrossRef]
36. Wang, S.S.; Zhao, W.X.; Qiu, T.Y.; Liu, W.L.; Yan, P.; Jiao, L.; Wang, X.B. Effect of cutting fluid on milled surface quality and tool life of aluminum alloy. *Materials* **2023**, *16*, 2198. [CrossRef]

37. Lin, H.M.; Liao, Y.S.; Wei, C.C. Wear behavior in turning high hardness alloy steel by CBN tool. *Wear* **2008**, *264*, 679–684. [CrossRef]
38. Axinte, D.A.; Belluco, W.; Chiffre, L.D. Reliable tool life measurements in turning- an application to cutting fluid efficiency evaluation. *Int. J. Mach. Tools Manuf.* **2001**, *41*, 1003–1014. [CrossRef]
39. Sun, S.; Fu, H.; Ping, X.; Lin, J.; Lei, Y.; Wu, W.; Zhou, J. Reinforcing behavior and microstructure evolution of NbC in laser cladding Ni45 coating. *Appl. Surf. Sci.* **2018**, *455*, 160–170. [CrossRef]
40. Naskar, A.; Chattopadhyay, A.K. Investigation on flank wear mechanism of CVD and PVD gard coating in high speed dry turning of low and high carbon steel. *Wear* **2018**, *396–397*, 98–106. [CrossRef]